Journal of
Materials Chemistry A

ROYAL SOCIETY
OF CHEMISTRY

COMMUNICATION

View Article Online
View Journal | View Issue

Cite this: *J. Mater. Chem. A*, 2020, **8**, 1131

Received 17th November 2019
Accepted 8th December 2019

DOI: 10.1039/c9ta12605h

rsc.li/materials-a

A chlorinated nonacyclic carbazole-based acceptor affords over 15% efficiency in organic solar cells†

Tsung-Wei Chen,[ad] Kuan-Lin Peng,[ad] You-Wei Lin,[ad] Yi-Jia Su,[ad] Ko-Jui Ma,[ad] Ling Hong,[bc] Chia-Chih Chang,[ad] Jianhui Hou*[bc] and Chain-Shu Hsu*[ad]

In this contribution, a dithienocyclopentacarbazole (DTC)-based and two dithieno[3,2-*b*]thiophenecyclopentacarbazole (DTTC)-based non-fullerene acceptors (NFAs) named DTC-4F, DTTC-4F and DTTC-4Cl were exploited to elucidate the effects of conjugation extension and end group chlorination. DTTC-4F was designed through conjugation extension on the basis of DTC-4F by fusing one additional thiophene on both flanks of the heptacyclic DTC core, generating the nonacyclic DTTC core. Compared with DTC-4F, DTTC-4F features up-shifted energy levels, red-shifted absorption and enhanced π–π interaction. PM6:DTTC-4F exhibits a decent PCE of 13.89% with a V_{OC} of 0.95 V, a J_{SC} of 21.66 mA cm^{-2} and a FF of 67.60%. Although DTTC-4F affords a reduced FF compared to DTC-4F, a DTTC-4F-based device delivers a higher PCE than DTC-4F-based devices due to the extended absorption range of DTCC-4F in comparison with DTC-4F. Since chlorinated NFAs are known to possess stronger π–π interaction than fluorinated NFAs, DTTC-4Cl was therefore synthesized by end-capping DTTC core with 2Cl-IC groups instead of 2F-IC groups. Moreover, DTTC-4Cl demonstrates a red-shifted absorption in comparison with DTTC-4F, which is beneficial for light-harvesting. Overall, PM6:DTTC-4Cl affords an outstanding PCE of 15.42% with a V_{OC} of 0.92 V, a J_{SC} of 22.64 mA cm^{-2} and a FF of 74.04%, which is the record PCE observed in carbazole-based NFAs.

Introduction

Bulk-heterojunction (BHJ) organic solar cells (OSCs) have received increasing attention in solution-processable photovoltaic technology owing to their versatile merits of flexibility, transparency, and light weight.[1–3] In recent years, non-fullerene acceptors (NFAs) have emerged as a promising alternative to their fullerene counterparts because NFAs are capable of overcoming several intrinsic flaws of fullerene derivatives, such as weak and narrow absorption, limited energy level variability and thermally induced aggregation.[4] Fullerene derivatives are capable of affording a power-conversion efficiency (PCE) of around 10% whereas current state-of-the-art NFAs enable a PCE of 16.5% in binary OSCs and 17.3% in tandem OSCs in conjunction with high performance donors.[5–7] PM6 (also known as PBDB-TF), whose structure is shown in Fig. 1(a), is one of the most commonly utilized donors with high performance owing to its low-lying energy levels and strong absorption.[8–10] The prominent performances of PM6 in literature precedents are summarized in Fig. 1(b).[11–19] This representative trade-off relationship between open-circuit voltage (V_{OC}) and short-circuit current (J_{SC}) indicates that sacrificing V_{OC} to improve J_{SC} is an effective strategy to enhance PCE. Therefore, it is imperative to develop NFAs affording high J_{SC} performance through molecular engineering.

Rational molecular design of NFAs provides an opportunity to construct high performance OSCs. In particular, the use of an acceptor–donor–acceptor (A–D–A) scaffold in which the ladder-type donor core is end-capped with two highly electron-deficient motifs is now regarded as the most successful strategy to afford high performance NFAs. On the basis of the A–D–A scaffold, versatile strategies have been developed to improve photovoltaic performance.[20–23] In order to promote J_{SC} performance, conjugation extension and end group chlorination are both effective approaches mentioned in literature precedents[6,24–28] and Table S1.† The following NFAs with their structures shown in Fig. S1† are exploited to study the effects of extended conjugation and chlorination. For example, Zhan and coworkers reported an undecacyclic NFA, IUIC, by extending the π-conjugation of the heptacyclic core of ITIC4 (also known as IT-4F) with additional fused thiophene.[27]

---

[a] Department of Applied Chemistry, National Chiao Tung University, 1001 University Rd, Hsinchu 30010, Taiwan. E-mail: cshsu@mail.nctu.edu.tw

[b] State Key Laboratory of Polymer Physics and Chemistry, Beijing National Laboratory for Molecular Sciences Institute of Chemistry, Chinese Academy of Sciences, Beijing 100190, P. R. China. E-mail: hjhzlz@iccas.ac.cn

[c] University of Chinese Academy of Sciences, Beijing 100049, P. R. China

[d] Center for Emergent Functional Matter Science, National Chiao Tung University, 1001 University Rd, Hsinchu 30010, Taiwan

† Electronic supplementary information (ESI) available. See DOI: 10.1039/c9ta12605h

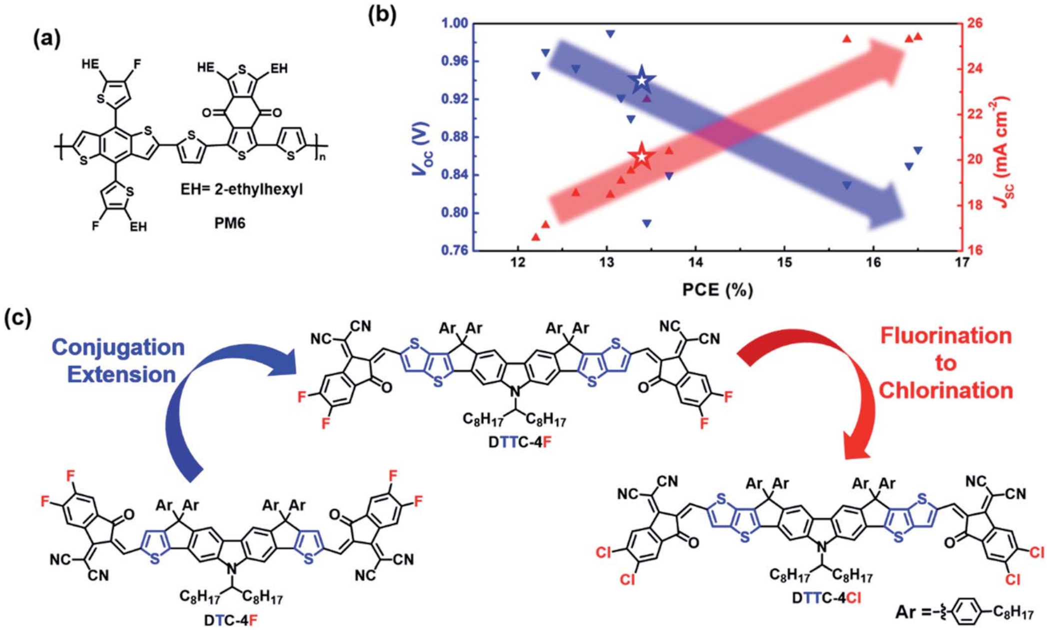

Fig. 1 (a) Chemical structure of PM6; (b) statistic diagram of PM6-based OSCs where "blue" represents the V_{OC} value and "red" represents the J_{SC} value. Specifically, PM6:DTC-4F-based photovoltaic performances were noted as the presence of "star"; (c) chemical structures of DTC-4F, DTTC-4F and DTTC-4Cl.

Compared with ITIC4, IUIC exhibits a red-shifted absorption, which could contribute to higher J_{SC} values. More importantly, the IUIC-based OSCs demonstrate a decent PCE of 11.20% with a high J_{SC} of 21.74 mA cm^{-2} whereas the ITIC4-based OSCs demonstrate a PCE of 8.18% with a J_{SC} of 16.66 mA cm^{-2}. Also, Yang and coworkers reported an octacyclic NFA called IDT8CN-M and a hexacyclic NFA, IDT6CN-M.[26] The IDT8 core features an additional thienothiophene unit fused on the IDT6 core, which extends the π-conjugation. Therefore, IDT8CN-M exhibits a red-shifted absorption compared to IDT6CN-M. Compared with IDT6CN-M-based OSCs, the IDT8CN-M-based OSCs afford an improved J_{SC} from 15.97 to 17.11 mA cm^{-2} with enhanced PCE from 11.23% to 12.43%. To this end, conjugation extension is indeed a powerful strategy in improving both J_{SC} and PCE. On the other hand, Forrest and coworkers have synthesized a chlorinated NFA, BT-CIC, with extra chlorine atoms on the both ends of its non-chlorinated counterpart, BT-IC.[28] BT-CIC shows a red-shifted absorption relative to BT-IC, resulting in an improved J_{SC} from 17.5 to 22.5 mA cm^{-2} and a higher PCE from 8.3% to 11.2% in the corresponding devices. In addition, Hou and coworkers have reported a chlorinated NFA named BTP-4Cl (also known as Y7) and compared its photovoltaic performance with that of the fluorinated NFA, BTP-4F (also known as Y6).[6] BTP-4Cl shows a red-shifted absorption than BTP-4F, affording an increased J_{SC} from 24.9 to 25.4 mA cm^{-2} with improved PCE from 15.6% to 16.5%.

Our previous efforts have created numerous fused-ring structures and interfacial materials through molecular design.[8,11,22,29–36] Very recently, DTC-4F (previously named DTC(4Ph)-4FIC) afforded a decent PCE of 13.36% with a V_{OC} of 0.94 V, a J_{SC} of 20.20 mA cm^{-2} and a FF of 70.42%.[11] As observed in Fig. 1(b), the J_{SC} performance of the PM6:DTC-4F device is lagging behind relative to several high-performance devices. We then designed DTTC-4F with the structure shown in Fig. 1(c), featuring a nonacyclic DTTC core end-capped with 2F-IC terminal groups, where we attempt to broaden the absorption range to the near-infrared region. Coincidently, during the preparation of this manuscript, Tang *et al.* reported a nonacylclic NFA called CZTT-4F featuring small variation with DTTC-4F in structure.[37] CZTT-4F is designed with four 4-hexaphenyl side chains at the sp^3 carbons and a branched 2-ethylhexyl side chain at the nitrogen whereas DTTC-4F contains four 4-octaphenyl side chains at the sp^3 carbons and a branched 1-octylnonayl side chain at the nitrogen. Such a slight difference between CZTT-4F and DTTC-4F presumably manifests similar optical and electronic properties. However, the longer side chains of DTTC-4F provide more steric hindrance with respect to CZTT-4F, which may reduce the intermolecular interaction and suppress severe self-aggregation potentially. Furthermore, the merits of the DTTC core motivate us to develop NFAs with more red-shifted absorption. DTTC-4Cl, whose structure is shown in Fig. 1(c), is therefore synthesized, retaining the DTTC core but end-capped with 2Cl-IC terminal groups instead. Overall, DTTC-4F-based devices exhibit an impressive PCE of 13.89% with a V_{OC} of 0.95 V, a J_{SC} of 21.66 mA cm^{-2} and a FF of 67.60%. Moreover, DTTC-4Cl-based devices afford a remarkable PCE of 15.42% with a V_{OC} of 0.92 V, a J_{SC} of 22.64 mA cm^{-2} and a FF of 74.04%, which is the best photovoltaic performance observed in carbazole-based NFAs.[11,29,37–39]

Results and discussion

PM6 was synthesized on the basis of our previous contribution and analyzed by high temperature gel permeation chromatography, as shown in Fig. S3.† DTC-4F was synthesized and characterized according to our previous work and the synthetic scheme of DTTC-4F and DTTC-4Cl is shown in Fig. S4.†[11] DTTC-4F and DTTC-4Cl were synthesized using an end-capping DTTC core with 2F-IC/2Cl-IC through Knoevenagel condensation and the structures are fully confirmed by high-resolution mass spectrometry (HRMS) and ^{1}H/^{13}C NMR, as shown in Fig. S5 and S6.† DTTC-4F and DTTC-4Cl exhibit decent solubility in commonly used solvents including chloroform, chlorobenzene and *o*-dichlorobenzene, which is essential for solution-processed device fabrication. On the other hand, the thermal properties of DTTC-4F and DTTC-4Cl were characterized by thermogravimetric analysis (TGA), as shown in Fig. S7.† DTTC-4F and DTTC-4Cl manifest excellent thermal stability with high decomposition temperatures (T_d) of 337 and 338 °C, respectively. As characterized by differential scanning calorimetry (DSC), as shown in Fig. S8,† both DTTC-4F and DTTC-4Cl exhibit their amorphous nature.

To evaluate the highest occupied molecular orbital (HOMO)/the lowest unoccupied molecular orbital (LUMO) of DTC-4F, DTTC-4F and DTTC-4Cl, density functional theory (DFT) calculations at the B3LYP/6-31G(d,p) level were carried out, as shown in Fig. 2. The HOMO/LUMO generated from theoretical calculation of DTC-4F, DTTC-4F and DTTC-4Cl is −5.76/−3.66, −5.69/−3.61 and −5.72/−3.67 eV, respectively. Compared with DTC-4F, DTTC-4F exhibits an up-shifted HOMO/LUMO, which can be ascribed to the stronger electron-donating characteristic of the DTTC core than the DTC core. Also, since 2Cl-IC features stronger electron-withdrawing ability than 2F-IC, DTTC-4Cl exhibits a down-shifted HOMO/LUMO in comparison with DTTC-4F. Besides, as obtained from DFT calculation, the bandgaps of DTC-4F, DTTC-4F and DTTC-4Cl are 2.10, 2.08 and 2.05 eV, respectively. According to the electron distribution of HOMO/LUMO as shown in Fig. 2, it is unambiguous that such heptacyclic and nonacyclic A–D–A structures facilitate delocalization of π-electrons, ensuring efficient intramolecular charge transfer (ICT).

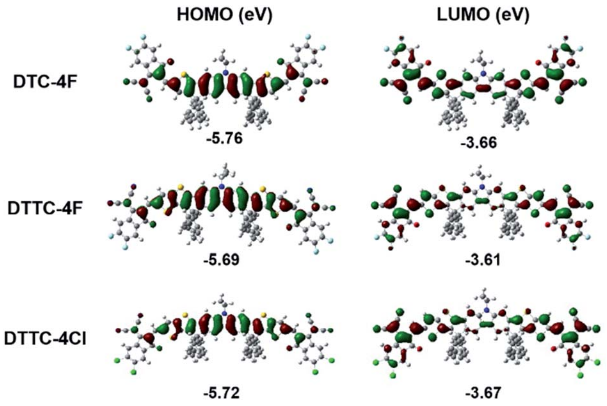

Fig. 2 Electron distribution and geometry simulation calculated through the B3LYP density function with a 6-31G(d,p) basis set in the HOMO/LUMO of DTC-4F, DTTC-4F and DTTC-4Cl.

The UV-vis absorption spectra of DTC-4F, DTTC-4F and DTTC-4Cl in dilute dichloromethane solution are shown in Fig. 3(a). As shown in Table 1, the extinction coefficient ($\varepsilon_{\max}$) of DTC-4F, DTTC-4F and DTTC-4Cl is 2.18 × 10^5, 2.20 × 10^5 and 2.36 × 10^5 M^{-1} cm^{-1}, respectively. Compared with DTC-4F, DTTC-4F exhibits a comparable $\varepsilon_{\max}$ value whereas DTTC-4Cl exhibits a higher $\varepsilon_{\max}$ value of *ca.* 8.3%, indicating their strong ICT characteristics. We envisaged that such an increment in ICT observed from DTTC-4Cl can be attributed to the strong electron-donating DTTC core and the strong electron-withdrawing 2Cl-IC end groups, which is consistent with the results obtained from the DFT calculation. Also, the normalized absorption spectra of DTC-4F, DTTC-4F and DTTC-4Cl in the film are shown in Fig. 3(b). The absorption peaks in the solution/film of DTC-4F, DTTC-4F and DTTC-4Cl are located at 672/701, 676/725 and 690/753 nm, respectively. Compared with DTC-4F, DTTC-4F exhibits red-shifted solution/film absorptions whereas DTTC-4Cl exhibits more red-shifted absorption than DTTC-4F. The optical bandgap (E_g^{Opt}), obtained from $E_g^{\mathrm{Opt}} = 1240/\lambda_{\mathrm{onset}}^{\mathrm{film}}$, of DTC-4F, DTTC-4F and DTTC-4Cl is 1.63, 1.55 and 1.47 eV. In addition, schematic energy level diagrams are illustrated in Fig. 3(c) where the HOMO/LUMO is acquired from cyclic voltammetry (CV) measurement, as shown in Fig. S10.† Similar to the results of DFT simulation, the HOMO/LUMOs of DTC-4F, DTTC-4F and DTTC-4Cl are −5.79/−3.92, −5.69/−3.91 and

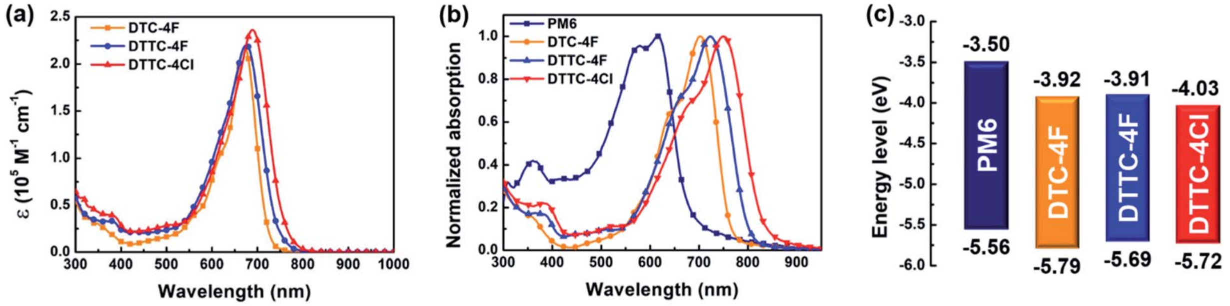

Fig. 3 (a) UV-vis absorption spectra obtained in dilute dichloromethane solution; (b) normalized UV-vis absorption spectra in the film; (c) schematic energy level diagrams of PM6, DTC-4F, DTTC-4F and DTTC-4Cl.

Table 1 Optical and electronic properties of DTC-4F, DTTC-4F and DTTC-4Cl

NFA	$\lambda_{\max}^{\text{sol}}$ [nm]	$\lambda_{\max}^{\text{film}}$ [nm]	$\varepsilon_{\max}{}^{a}$ [10^5 M^{-1} cm^{-1}]	E_g^{Opt} [eV]	HOMO^b [eV]	LUMO^b [eV]
DTC-4F	672	701	2.18	1.63	−5.79	−3.92
DTTC-4F	676	725	2.20	1.55	−5.69	−3.91
DTTC-4Cl	690	753	2.36	1.47	−5.72	−4.03

[a] Extinction coefficient was measured in dilute dichloromethane solution. [b] HOMO/LUMO was evaluated through cyclic voltammetry measurement.

−5.72/−4.03 eV. It is noteworthy that DTC-4F, DTTC-4F and DTTC-4Cl exhibit complementary absorptions and a well-matched HOMO/LUMO with PM6, which satisfy the prerequisites to construct high performance OSCs.

With illustration of the inverted OSC shown in Fig. 4(a), photovoltaic performances were characterized in a device structure of ITO/ZnO/C-PCBSD/active layer/MoO_3/Al. The C-PCBSD interlayer with its structure shown in Fig. S2.† is capable of affording extra exciton dissociation and better J_{SC} performance as observed in literature precedents.[11,31,32,35] The current density *vs.* voltage (*J–V*) curves of PM6:DTC-4F, PM6:DTTC-4F and PM6:DTTC-4Cl are shown in Fig. 4(b) whereas the photovoltaic parameters are summarized in Table 2. The PM6:DTTC-4F-based device delivers an impressive PCE of 13.89% with a V_{OC} of 0.95 V, a J_{SC} of 21.66 mA cm^{-2} and a FF of 67.60%. Compared with the PM6:DTC-4F-based device, the improved V_{OC} and J_{SC} performance of the PM6:DTTC-4F-based device benefits from the up-shifted LUMO and red-shifted absorption of DTTC-4F relative to DTC-4F. Although a decreased FF value from 70.42% to 67.60% is obtained, the PCE improves from 13.37% to 13.89% for the DTTC-4F-based device with respect to the DTC-4F-based device. For the PM6:DTTC-4Cl-based device, a remarkable PCE of 15.42% is achieved with a V_{OC} of 0.92 V, a J_{SC} of 22.64 mA cm^{-2} and a FF of 74.04%. Because of the down-shifted LUMO of DTTC-4Cl, the PM6:DTTC-4Cl device exhibits a decreased V_{OC} performance from 0.95 to 0.92 V in comparison with the PM6:DTTC-4F-based device. However, the energy loss (E_{loss}) of PM6:DTC-4F, PM6:DTTC-4F and PM6:DTTC-4Cl devices is 0.68, 0.60 and 0.55 eV, respectively. The suppressed E_{loss} value is advantageous to afford decent V_{OC} performance and an E_{loss} of 0.55 eV is comparable to other high-performance binary OSCs.[6,12,16,18] In addition, the increment of J_{SC} and FF performance in the PM6:DTTC-4Cl-based device can be attributed to the red-shifted absorption and reinforced ICT characteristic of DTTC-4Cl with respect to DTTC-4F. The systematic molecular modification including conjugation extension and end group chlorination proves effective in boosting both J_{SC} and PCE. To carefully evaluate the J_{SC} performance, the external quantum efficiency (EQE) measurements of the devices containing DTC-4F, DTTC-4F and DTTC-4Cl are conducted. As confirmed by the blend absorption shown in Fig. S11,† PM6:DTC-4F, PM6:DTTC-4F and PM6:DTTC-4Cl exhibit consistent onsets with the EQE spectrum shown in Fig. 4(c). The current density values integrated from EQE spectra ($J_{\text{Calc.}}$) are summarized in Table 2, confirming the validity of the J_{SC} results obtained from the *J–V* curves. Owing to the red-shifted absorption of DTTC-4F and DTTC-4Cl, the PM6:DTTC-4F and PM6:DTTC-4Cl-based devices afford $J_{\text{Calc.}}$s of 19.48 and 21.53 mA cm^{-2} whereas the PM6:DTC-4F-based device exhibits a $J_{\text{Calc.}}$ of 18.57 mA cm^{-2}.

Space-charge limited current (SCLC) measurement is exploited to gain insight into the exciton transportation of the PM6:DTC-4F, PM6:DTTC-4F and PM6:DTTC-4Cl blends. Electron-only devices of ITO/ZnO/active layer/Al and hole-only devices of ITO/PEDOT:PSS/active layer/Au are utilized to measure the electron/hole mobility. As characterized in Fig. S12† and summarized in Table S2,† PM6:DTC-4F, PM6:DTTC-4F and PM6:DTTC-4Cl devices exhibit electron/hole mobility of $3.51 \times 10^{-4}/2.56 \times 10^{-4}$, $3.02 \times 10^{-4}/2.70 \times 10^{-4}$ and $7.91 \times 10^{-4}/6.22 \times 10^{-4}$ cm^2 V^{-1} s^{-1}, respectively. Among these three binary blends, PM6:DTTC-4Cl exhibits the fastest electron/hole mobility, which is consistent with its

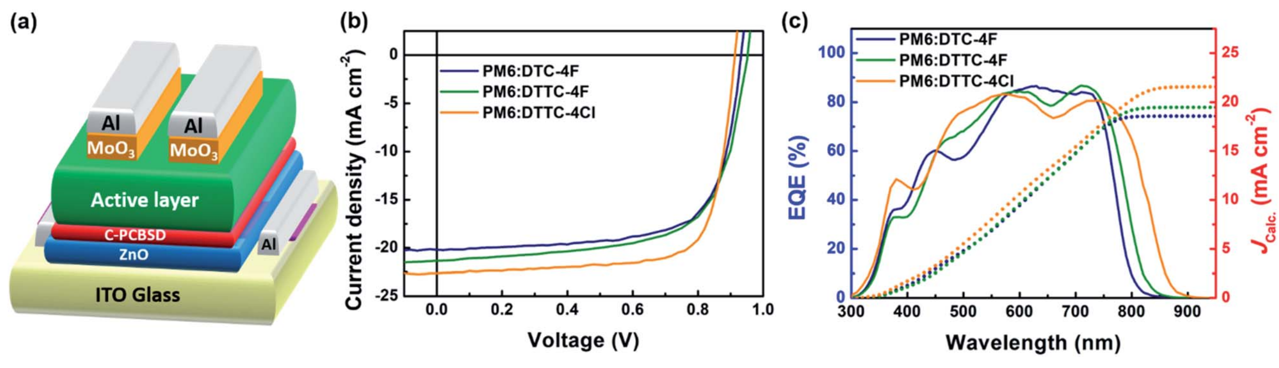

Fig. 4 (a) Illustration of the inverted OSC; (b) *J–V* characteristics under simulated AM 1.5 G irradiation (100 mW cm^{-2}) and (c) EQE spectra with integrated $J_{\text{Calc.}}$ curves.

Table 2 Optimized photovoltaic performance of OSCs containing DTC-4F, DTTC-4F and DTTC-4Cl

Device	$V_{OC}{}^{a}$ $(V_{OC})^{b}$ [V]	$J_{SC}{}^{a}$ $(J_{SC})^{b}$ [mA cm^{-2}]	$J_{Calc.}{}^{c}$ [mA cm^{-2}]	FF^{a} (FF)^{b} [%]	PCE^{a} (PCE)^{b} [%]	$E_{loss}{}^{d}$ [eV]
PM6:DTC-4F	0.94 (0.94 ± 0.01)	20.20 (19.94 ± 0.20)	18.57	70.42 (71.46 ± 0.85)	13.37 (13.00 ± 0.16)	0.68
PM6:DTTC-4F	0.95 (0.95 ± 0.01)	21.66 (21.45 ± 0.27)	19.48	67.60 (66.88 ± 0.74)	13.89 (13.57 ± 0.24)	0.60
PM6:DTTC-4Cl	0.92 (0.92 ± 0.01)	22.64 (22.36 ± 0.19)	21.53	74.04 (74.14 ± 0.84)	15.42 (15.02 ± 0.19)	0.55

[a] Photovoltaic performance obtained from the best device. [b] Photovoltaic performance averaged from over 10 devices with their standard deviation. [c] Current density calculated from EQE measurement. [d] E_{loss} evaluated using $E_{loss} = E_g - eV_{OC}$.

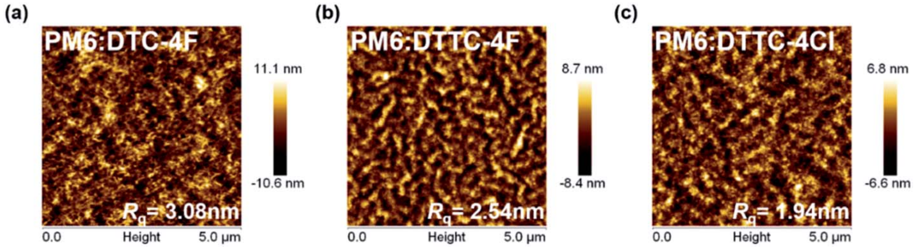

Fig. 5 AFM height images of (a) PM6:DTC-4F, (b) PM6:DTTC-4F and (c) PM6:DTTC-4Cl blends.

high FF. Also, PM6:DTTC-4F exhibits a decreased electron mobility with respect to PM6:DTC-4F and PM6:DTTC-4Cl, which may be responsible for its relatively low FF of 67.60% to some extent.

Because non-radiative energy loss (ΔE_3) plays a significant role in maintaining the V_{OC} performance,[6] EQE$_{EL}$ measurements of PM6:DTC-4F, PM6:DTTC-4F and PM6:DTTC-4Cl are carried out, as shown in Fig. S13† with EQE$_{EL}$ and ΔE_3 summarized in Table S3.† High EQE$_{EL}$ values and low ΔE_3 are favourable to afford decent V_{OC} performance. PM6:DTC-4F, PM6:DTTC-4F and PM6:DTTC-4Cl exhibit their EQE$_{EL}$ values with a magnitude of 10^{-5} and the representative ΔE_3 is 0.289, 0.267 and 0.269 eV, respectively. DTTC-4F and DTTC-4Cl-based devices afford reduced ΔE_3 compared to DTC-4F-based devices, indicating that DTTC-4F and DTTC-4Cl are more capable of maintaining their V_{OC} performance than DTC-4F when a non-radiative mechanism dominates. As a result, it is inferred that conjugation extension could effectively decrease ΔE_3. Also, PM6:IT-4F and PM6:Y6, two of the state-of-the-art binary systems, are characterized, which exhibit EQE$_{EL}$ values with magnitude of 10^{-6} (PM6:IT-4F) and magnitude of 10^{-4} (PM6:Y6). It is noteworthy that the EQE$_{EL}$ values of DTC-4F, DTTC-4F and DTTC-4Cl are an order of magnitude higher than those of IT-4F but an order of magnitude lower than those of Y6 in the PM6-based binary system.

To probe the morphology and phase separation of active layers, atomic force microscopy (AFM) and transmission electron microscopy (TEM) measurements were carried out, as shown in Fig. 5 and S14.† The root-mean-square roughness (R_q) obtained from PM6:DTC-4F, PM6:DTTC-4F and PM6:DTTC-4Cl thin films is 3.08, 2.54 and 1.94 nm, respectively. Compared with the PM6:DTC-4F thin film, more pronounced fibril interpenetrating frameworks with more distinct phase separation at the nanoscale can be observed in PM6:DTTC-4F and PM6:DTTC-4Cl blends.

To elucidate the extent of intermolecular interaction and packing alignment in thin films, grazing-incidence wide-angle X-ray scattering (GIWAXS) analysis was conducted. With 2D GIWAXS patterns characterized in Fig. S8,† the relevant *d*-spacing of DTTC-4F and DTTC-4Cl neat films is summarized in Table S4.† Similar to the DTC-4F neat film in our previous effort, the DTTC-4F and DTTC-4Cl neat films manifest face-on preferences whereas DTTC-4Cl exhibits a more pronounced (010) peak than DTTC-4F. Also, the (010) *d*-spacing of DTTC-4F and DTTC-4Cl neat films is 3.61 and 3.59 Å, which are smaller than 4.27 Å observed for the DTC-4F neat film, indicating their stronger π–π interaction. In addition, the 2D GIWAXS patterns of PM6:DTC-4F, PM6:DTTC-4F and PM6:DTTC-4Cl blends with

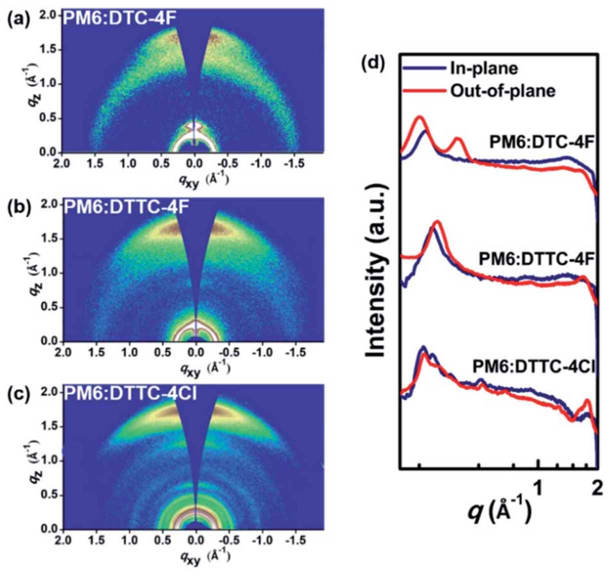

Fig. 6 2D GIWAXS patterns of (a) PM6:DTC-4F, (b) PM6:DTTC-4F and (c) PM6:DTTC-4Cl with (d) their corresponding 1D line cuts.

relevant 1D line cuts are displayed in Fig. 6. The PM6:DTC-4F, PM6:DTTC-4F and PM6:DTTC-4Cl blends exhibit face-on preference with (010) *d*-spacings of 3.87, 3.69 and 3.51 Å. Also, the π–π coherence length (CL) of PM6:DTC-4F, PM6:DTTC-4F and PM6:DTTC-4Cl blends is 26.27, 30.20 and 43.33 Å. Benefiting from the strong π–π interaction as observed in DTTC-4F and DTTC-4Cl neat films, PM6:DTTC-4F and PM6:DTTC-4Cl blends manifest enhanced π–π interaction and more ordered packing than PM6:DTC-4F, which is advantageous for charge transport and thus increases the mobility.

Conclusion

In this contribution, we exploit DTC-4F, DTTC-4F and DTTC-4Cl as non-fullerene acceptors (NFAs) to elucidate the effect of conjugation extension and end group chlorination. Compared with DTC-4F, DTTC-4F features up-shifted energy levels, red-shifted absorption and enhanced π–π interaction. PM6:DTTC-4F exhibits a decent PCE of 13.89% with a V_{OC} of 0.95 V, a J_{SC} of 21.66 mA cm^{-2} and a FF of 67.60%. Moreover, DTTC-4Cl demonstrates a red-shifted absorption in comparison with DTTC-4F, which is beneficial for light-harvesting. The PM6:DTTC-4Cl blend manifests the smoothest surface with strongest π–π interaction in comparison with the PM6:DTC-4F and PM6:DTTC-4F blends, indicating its capability to deliver a decent FF. Overall, PM6:DTTC-4Cl affords an outstanding PCE of 15.42% with a V_{OC} of 0.92 V, a J_{SC} of 22.64 mA cm^{-2} and a FF of 74.04%. In addition, PM6:DTTC-4F and PM6:DTTC-4Cl feature reduced ΔE_3 with respect to PM6:DTC-4F, indicating that conjugation extension is effective in decreasing ΔE_3. Our effort provides a systematic approach to boost both J_{SC} and PCE, leading to the record photovoltaic performance observed in carbazole-based OSCs.

Conflicts of interest

There are no conflicts to declare.

Acknowledgements

This work was supported by the Ministry of Science and Technology, Taiwan (grant No. MOST107-3017-F009-003) and the Center for Emergent Functional Matter Science of National Chiao Tung University from The Featured Areas Research Center Program within the framework of the Higher Education Sprout Project by the Ministry of Education (MOE) in Taiwan. Also, we are grateful to the National Center for High-performance Computing for computer time and facilities.

Notes and references

1 J.-S. Wu, S.-W. Cheng, Y.-J. Cheng and C.-S. Hsu, *Chem. Soc. Rev.*, 2015, **44**, 1113–1154.
2 Y. Li, *Acc. Chem. Res.*, 2012, **45**, 723–733.
3 Y.-J. Cheng, S.-H. Yang and C.-S. Hsu, *Chem. Rev.*, 2009, **109**, 5868–5923.
4 Y. Lin, J. Wang, Z. G. Zhang, H. Bai, Y. Li, D. Zhu and X. Zhan, *Adv. Mater.*, 2015, **27**, 1170–1174.
5 L. Meng, Y. Zhang, X. Wan, C. Li, X. Zhang, Y. Wang, X. Ke, Z. Xiao, L. Ding, R. Xia, H. L. Yip, Y. Cao and Y. Chen, *Science*, 2018, **361**, 1094–1098.
6 Y. Cui, H. Yao, J. Zhang, T. Zhang, Y. Wang, L. Hong, K. Xian, B. Xu, S. Zhang, J. Peng, Z. Wei, F. Gao and J. Hou, *Nat. Commun.*, 2019, **10**, 2515–2523.
7 Y. Liu, J. Zhao, Z. Li, C. Mu, W. Ma, H. Hu, K. Jiang, H. Lin, H. Ade and H. Yan, *Nat. Commun.*, 2014, **5**, 5293–5301.
8 Y. Wang, Q. Fan, X. Guo, W. Li, B. Guo, W. Su, X. Ou and M. Zhang, *J. Mater. Chem. A*, 2017, **5**, 22180–22185.
9 T. J. Aldrich, S. M. Swick, F. S. Melkonyan and T. J. Marks, *Chem. Mater.*, 2017, **29**, 10294–10298.
10 M. Zhang, X. Guo, W. Ma, H. Ade and J. Hou, *Adv. Mater.*, 2015, **27**, 4655–4660.
11 T.-W. Chen, C.-C. Chang, Y.-T. Hsiao, C. Chan, L. Hong, L. Zhong, W.-T. Chuang, J. Hou, Y. Li and C.-S. Hsu, *ACS Appl. Mater. Interfaces*, 2019, **11**, 31069–31077.
12 H. Feng, Y. Q. Q. Yi, X. Ke, J. Yan, Y. Zhang, X. Wan, C. Li, N. Zheng, Z. Xie and Y. Chen, *Adv. Energy Mater.*, 2019, **9**, 1803541.
13 W. Li, L. Ye, S. Li, H. Yao, H. Ade and J. Hou, *Adv. Mater.*, 2018, **30**, 1707170.
14 Y. Jia, Y. Zhang, W. Jiang, B. Su, C. Liu, E. Zhu and G. Che, *J. Mater. Chem. A*, 2019, **7**, 10905–10911.
15 S. Li, L. Ye, W. Zhao, X. Liu, J. Zhu, H. Ade and J. Hou, *Adv. Mater.*, 2017, **29**, 1704051.
16 L. Hong, H. Yao, Z. Wu, Y. Cui, T. Zhang, Y. Xu, R. Yu, Q. Liao, B. Gao, K. Xian, H. Y. Woo, Z. Ge and J. Hou, *Adv. Mater.*, 2019, **31**, 1903441.
17 T. Liu, Z. Luo, Q. Fan, G. Zhang, L. Zhang, W. Gao, X. Guo, W. Ma, M. Zhang, C. Yang, Y. Li and H. Yan, *Energy Environ. Sci.*, 2018, **11**, 3275–3282.
18 J. Yuan, Y. Zhang, L. Zhou, G. Zhang, H.-L. Yip, T.-K. Lau, X. Lu, C. Zhu, H. Peng, P. A. Johnson, M. Leclerc, Y. Cao, J. Ulanski, Y. Li and Y. Zou, *Joule*, 2019, **3**, 1140–1151.
19 H. Zhang, H. Yao, J. Hou, J. Zhu, J. Zhang, W. Li, R. Yu, B. Gao, S. Zhang and J. Hou, *Adv. Mater.*, 2018, **30**, 1800613.
20 S. Dai, F. Zhao, Q. Zhang, T. K. Lau, T. Li, K. Liu, Q. Ling, C. Wang, X. Lu, W. You and X. Zhan, *J. Am. Chem. Soc.*, 2017, **139**, 1336–1343.
21 B. Fan, D. Zhang, M. Li, W. Zhong, Z. Zeng, L. Ying, F. Huang and Y. Cao, *Sci. China: Chem.*, 2019, **62**, 1869–1870.
22 C.-H. Li, C.-C. Chang, Y.-H. Hsiao, S.-H. Peng, Y.-J. Su, S. W. Heo, K. Tajima, M.-C. Tsai, C.-Y. Lin and C.-S. Hsu, *ACS Appl. Mater. Interfaces*, 2019, **11**, 1156–1162.
23 W. Zhao, S. Li, H. Yao, S. Zhang, Y. Zhang, B. Yang and J. Hou, *J. Am. Chem. Soc.*, 2017, **139**, 7148–7151.
24 B. Kan, H. Feng, H. Yao, M. Chang, X. Wan, C. Li, J. Hou and Y. Chen, *Sci. China: Chem.*, 2018, **61**, 1307–1313.
25 G. Cai, J. Zhu, Y. Xiao, M. Li, K. Liu, J. Wang, W. Wang, X. Lu, Z. Tang, J. Lian, P. Zeng, Y. Wang and X. Zhan, *J. Mater. Chem. A*, 2019, **7**, 21432–21437.
26 W. Gao, T. Liu, C. Zhong, G. Zhang, Y. Zhang, R. Ming, L. Zhang, J. Xin, K. Wu, Y. Guo, W. Ma, H. Yan, Y. Liu and C. Yang, *ACS Energy Lett.*, 2018, **3**, 1760–1768.

27 B. Jia, S. Dai, Z. Ke, C. Yan, W. Ma and X. Zhan, *Chem. Mater.*, 2017, **30**, 239–245.

28 Y. Li, J. D. Lin, X. Che, Y. Qu, F. Liu, L. S. Liao and S. R. Forrest, *J. Am. Chem. Soc.*, 2017, **139**, 17114–17119.

29 T.-W. Chen, Y.-T. Hsiao, Y.-W. Lin, C.-C. Chang, W.-T. Chuang, Y. Li and C.-S. Hsu, *Mater. Chem. Front.*, 2019, **3**, 829–835.

30 J.-S. Wu, Y.-J. Cheng, M. Dubosc, C.-H. Hsieh, C.-Y. Chang and C.-S. Hsu, *Chem. Commun.*, 2010, **46**, 3259–3261.

31 Y.-H. Chao, Y.-Y. Huang, J.-Y. Chang, S.-H. Peng, W.-Y. Tu, Y.-J. Cheng, J. Hou and C.-S. Hsu, *J. Mater. Chem. A*, 2015, **3**, 20382–20388.

32 Y.-J. Cheng, C.-H. Hsieh, P.-J. Li and C.-S. Hsu, *Adv. Funct. Mater.*, 2011, **21**, 1723–1732.

33 Y.-J. Cheng, J.-S. Wu, P.-I. Shih, C.-Y. Chang, P.-C. Jwo, W.-S. Kao and C.-S. Hsu, *Chem. Mater.*, 2011, **23**, 2361–2369.

34 Y.-T. Hsiao, C.-H. Li, S.-L. Chang, S. Heo, K. Tajima, Y.-J. Cheng and C.-S. Hsu, *ACS Appl. Mater. Interfaces*, 2017, **9**, 42035–42042.

35 Y.-Y. Lai, Y.-J. Cheing and C.-S. Hsu, *Energy Environ. Sci.*, 2014, **7**, 1866–1883.

36 J.-S. Wu, Y.-J. Cheng, T.-Y. Lin, C.-Y. Chang, P.-I. Shih and C.-S. Hsu, *Adv. Funct. Mater.*, 2012, **22**, 1711–1722.

37 H. Wang, Z. Zhang, J. Yu, X. Liu, S. Qu, S. Guang and W. Tang, *J. Mater. Chem. A*, 2019, **7**, 21903–21910.

38 Q. Tu, Y. Ma, X. Zhou, W. Ma and Q. Zheng, *Chem. Mater.*, 2019, **31**, 5953–5963.

39 X. Chen, H. Liu, L. Xia, T. Hayat, A. Alsaedi and Z. Tan, *Chem. Commun.*, 2019, **55**, 7057–7060.